Microchimica Acta
https://doi.org/10.1007/s00604-018-3141-7

ORIGINAL PAPER

A glassy carbon electrode modified with TiO_2(200)-rGO hybrid nanosheets for aptamer based impedimetric determination of the prostate specific antigen

Masoud Karimipour[1] · Esmaeil Heydari-Bafrooei[2] · Mahjubeh Sanjari[1] · Malin B. Johansson[3] · Mehdi Molaei[1]

Received: 4 September 2018 / Accepted: 1 December 2018

Abstract

TiO_2(200)-rGO hybrid nanosheets were synthesized starting from TiO_2, rGO and NaOH solid powders via a scalable hydrothermal process. The weight ratio of TiO_2-GO was found to be crucial on the crystal growth and biosensor properties of the final hybrid nanosheets. They were characterized by means of SEM, FESEM-EDX, XRD, XPS, Raman and FTIR spectroscopies in order to verify the formation of very thin TiO_2 anatase nanosheets with an orientation of the anatase crystal structure towards the (200) plane. The free active sites of TiO_2 structure and the large surface of the 2D graphene structure strongly facilitate charge transport confirmed by BET-BJH analyses. Compared to pure AuNPs, rGO and TiO_2, the hybrid nanosheet modified electrode represents the most sensitive aptasensing platform for the determination of PSA. The detection was based on that the variation of electron transfer resistance (Rct) at the modified electrode surface in a solution containing 3.0 mmol L^{-1} $[Fe(CN)_6]^{3-/4-}$ as a redox probe and 0.1 mol L^{-1} KCl as supporting electrolyte. The detection limit of the sensor is 1 pg mL^{-1}, and the sensor can be operated up to 30 days. It was applied to the analysis of PSA levels in spiked serum samples obtained from patients with prostate cancer. Data compare well with those obtained by an immunoradiometric assay.

Keywords Work function · X-ray photoelectron spectroscopy · Effective surface area · Aptasensor · Electrochemical impedance spectroscopy · Voltammetry

Introduction

Blood-based tumor markers are one of the most important approaches in the diagnosis of cancers, efficiency of drugs, monitoring of cancer progression and evaluation of resistance to chemotherapy [1, 2]. Tumour markers are commonly found at rather low levels in healthy persons [3]. As the tumor and metastases develop, the level changes, so clinical assays of cancer markers need to be fast, selective, and sensitive enough to detect small changes in the quantity of the biomarkers in complex biological fluids. Prostate specific antigen (PSA), a serine protease, is a widely used tumor marker to aid early detection of prostate cancer and evaluate the cancer progression in men with prostate cancer and to monitor treatment effects. Therefore, the detection of this glycoprotein is significant to diagnosis of prostate cancer and prevention of its progression [3]. Moreover, PSA is not only cancer-specific and therefore it is possible to be elevated in both malignant and benign conditions such as benign prostate hyperplasia [3]. The PSA concentration in men's serum is correlated with their age such that 1 ng mL^{-1} increases each 10 years. Thus for the sensitivity improvement and for the prediction of tumor aggressiveness and PCa morbidity, fast, low cost and more reliable analytical methods are needed [3]. Aptamer-based

Electronic supplementary material The online version of this article (https://doi.org/10.1007/s00604-018-3141-7) contains supplementary material, which is available to authorized users.

✉ Masoud Karimipour
m.karimipour@vru.ac.ir

✉ Esmaeil Heydari-Bafrooei
e.heydari@vru.ac.ir

[1] Department of Physics, Vali-e-Asr University of Rafsanjan, Rafsanjan 77139-36417, Iran

[2] Department of Chemistry, Faculty of Science, Vali-e-Asr University of Rafsanjan, Rafsanjan 77188–97111, Iran

[3] Department of Chemistry-Ångström, Physical Chemistry Uppsala University, 75120 Uppsala, Sweden

Published online: 18 December 2018

sensors (aptasensors) have attracted much attention in detecting PSA for clinical applications [4–7]. Aptamers can bind specifically to the target species (e.g., drugs, proteins, biomarkers, and other organic or inorganic molecules), that can be equivalent to those of antibodies as molecular recognition elements in biosensing application. Compared to optical aptasensors, electrochemical aptasensors are relatively simple in terms of instrumentation and analysis, reliability, low cost per assay, excellent sensitivity, short run time, potential for miniaturization, fast and real-time in situ analysis [8].

Rapid progress has been made in both aptasensor system developments and applications. For example, to increase the sensitivity of the electrochemical aptasensors, the researchers focus on emerging sensing materials. Materials including gold nanoparticles [9–11], molecularly-imprinted polymers [6], graphene [12] and carbon-nanotubes [13] have been developed to increase the surface area and improve the conductivity of electrodes, to enhance electrochemical signals from redox reactions, and finally to obtain sensitive detection of analyte. Current research is focused on the synthesis of scalable and cheap production of hybrid TiO_2-rGO nanosheets with superior physical properties which has been developed for aptamer-based electrochemical biosensing for the first time.

Experimental

For the details of synthesis of rGO-TiO_2 hybrid nanosheets and their structural, morphological and electronic characterization please see Electronic Supplementary Materials (ESM).

Chemicals

All solutions used in this work were prepared with reagent grade chemicals and doubly distilled water. PSA binding DNA aptamer (5′–TTT TTA ATT AAA GCT CGC CAT CAA ATA GCT TT-3′) was purchased from Bioneer (www.bioneer.com, Daejeon, Korea). PSA was obtained from Merck Chemicals Ltd., UK (www.merckmillipore.com). The Aptamer stock solutions were prepared in doubly distilled water and were stored at −4 °C. The electrolyte solution ($K_3[Fe(CN)_6]/K_4[Fe(CN)_6]$ mixture) was immediately prepared before use.

Electrochemical apparatus

All electrochemical measurements were performed using Autolab PGSTAT302N (https://www.metrohm-autolab.com) with NOVA 1.11 software (Eco Chemie, The Netherlands). This instrument was connected to three electrode cell containing modified glassy carbon electrode (GCE) as a working electrode, platinum as a counter electrode and Ag/AgCl (3 mol L^{-1} KCl) as a reference electrode.

Aptamer immobilization onto GO-TiO_2 and PSA detection

In order to construct the modified electrode, at first, glassy carbon electrode (GCE, 3.0 mm diameter, Metrohm) was polished with alumina powder (Aldrich, 0.1, 0.05 mm) using a Metrohm polishing kit for 5 min and then sonicated in water/ethanol solution (1:1 *v*/v) for 3 min. Finally, the GCE was dried under a continuous nitrogen stream at the room temperature. 5 μL nanocomposite dispersion was directly drop cast on the cleaned GCE and dried. The films were rinsed with water and dried too. In order to immobilize the aptamer on the surface of electrode, the modified GCE electrode with rGO-TiO_2 was immersed in 0.1 mol L^{-1} phosphate buffer containing aptamer (200 nM) for an immersion time of 9 h and then the film was rinsed with PBS to remove excess aptamer molecules.

Procedure

In order to measure the PSA using rGO-TiO_2/Apt/GCE, the modified electrode was prepared according to the recommended procedure in section 2.3. Then the rGO-TiO_2/Apt/GCE was transferred to electrochemical cell containing 5.0 mmol L^{-1} $[Fe(CN)_6]^{3-/4-}$ and differential pulse voltammetry (DPV) and electrochemical impedance spectroscopy (EIS) spectra was recorded to evaluate of I_1 and R_{ct} (R_1), respectively. In the next stage, the rGO-TiO_2/Apt/GCE was transferred to 0.1 mol L^{-1} phosphate buffer (pH = 7.0) containing different concentrations of PSA for 45 min under the stirring (400 rpm) and the DPV and EIS spectra were recorded again to measure I_2 and R_2, respectively. Ultimately I_2-I_1 and R_2-R_1/R_1 ($\Delta R/R1$) were considered as final signals. The calibration plot was obtained by plotting the $\Delta R/R_1$ against the concentration. Prior to measurement of PSA, all effective parameters in construction and measurement were evaluated and optimized. In the final stage, in order to assess the selectivity of our work, the effect of some compounds that are structurally similar to PSA was assessed and ultimately the amount of PSA in some real sample was measured.

Electrochemical impedance spectroscopy and voltammetry

Cyclic voltammetry (CV) and EIS measurements were performed in a solution containing 3.0 mmol L^{-1} $[Fe(CN)_6]^{3-/4-}$ as a redox probe and 0.1 mol L^{-1} KCl as supporting electrolyte. The EIS spectra were recorded in the frequency range of 0.005 to 10^5 Hz. The amplitude of the applied sine wave

potential in each case was 10 mV at a DC potential of +0.22 V (vs. Ag/AgCl). Operating conditions for DPV studies were: step potential of 8.0 mV; modulation amplitude of 50.0 mV (vs. Ag/AgCl); modulation time of 0.05 s and interval time of 0.5 s. All the electroanalytical measurements were performed at room temperature.

Sample preparation

Fresh Blood specimens of healthy and patient individuals were gifted by the Seyed-al-Shohada Hospital, Isfahan, Iran, and stored frozen until assay. The serum samples were separated and divided into two parts: first recognition by standard immunoradiometric assay and second recognition by the aptasensor. For the determination of PSA using the biosensor these samples were diluted with distilled water (1:9).

Results and discussion

Choice of the material

According to the explanation given in the introduction and considering benefits of the rGO and TiO_2 nanomaterials, we synthesized rGO-TiO_2 hybrid nanosheets and used them to construct the aptasensor in order to apply the synergy contributions on the enhancement of aptasensor characteristics. Compared with other electrochemical aptamer biosensors, the biosensor based on these nanomaterials has four advantages for biomolecule immobilization, including (i) large surface area, (ii) rich π –conjugation structure, and good in-plane conductivity due to presence of rGO, and (iii) a unique porous structure of TiO_2 nanosheets with large surface area and (iv) enhanced work function due to crystal texturing of TiO_2 that facilitates the charge transfer at the interface of TiO_2/rGO sheets.

Chemical components, morphology and crystal structure characterizations

The main idea of the formation of hybrid TiO_2-rGO nanosheets is based on Kasuga model of the formation of TiO2 nanotubes in hydrothermal procedure [14]. GO sheets are added to the procedure as template for sheet formation together with a careful change of $\frac{TiO_2}{GO}$ weight ratio. Only TiO_2 and GO powders are used in this approach. Hence, the weight ratio can be well controlled and tracked. For the formation of hybrid nanosheets based on Kasuga model, First TiO2 nanoparticles should dissociate to Ti-O-Na bonds through hydrothermal reactions [14] and then link to GO sheets through carboxyl and hydroxyl groups which means simultaneous reduction of GO to reduced-graphene oxide can also be observed. Fig. S1-Fig.S4 (See Electronic Supplementary Materials) reveal the quality of TiO_2 nanoparticles and GO powder were used for the synthesis of TiO_2-rGO hybrid nanosheets.

In most reports, the weight or molar ratio of $\frac{TiO_2}{GO}$ is much higher than unity such that graphene is considered as doping in TiO_2 matrix. But in this report, this ratio is kept below unity to investigate the real effect of proximity of wide band gap semiconductor on GO sheets. One of the very significant consequences of this choice, is the growth of TiO_2 anatase phase with new preferential growth plane of (200) as seen clearly from Fig.1. It demonstrates the XRD patterns of samples with different x: $\frac{TiO_2}{GO}$ weight ratios. For x = 1, both rutile and anatase phases are observed but for x < 1, only Single anatase phase of TiO_2 is observed. A significant shift of GO characteristic peak to lower angles ($2 \approx 10°$) is observed. This is due to the growth of TiO_2 sheets between GO layers which results in the increase of interlayer spacing of GO sheets. To examine this idea, SEM (Fig. S5), micrograph (Fig. S6) and FESEM (Fig. S7, Fig. S8) images for the samples were obtained. The results show a layered structure at nanoscales containing TiO_2 nanosheets conjugated with reduced graphene oxide sheets. Raman spectroscopy (Fig. S9) prove that with the increase of GO powder, graphene structure dominates and the density of defects are highly influenced by $\frac{TiO_2}{GO}$ weight ratio (see Electronic Supplemetary materials for details). EDS results (Fig. S10 and Fig. S11) indicate that the compositional change of $\frac{TiO_2}{GO}$ weight ratio in hybrid nanosheets is qualitatively and quantitatively predictable via only adjustment of initial TiO_2 and GO weight powders.

To scrutinize the electronic states of hybrid nanosheets, XPS analysis has been conducted for S5 as depicted in Fig. 2. C1s orbital scan (Fig. 2b) shows the presence of C-C/C=C at 284.9 eV binding as well as a satellite peak at 286.7 eV related to Ti-O-C (C-O) bond. It is an indication of hybridization of rGO and TiO_2 [15]. Moreover Fig. 2d shows the presence of two types of oxygen bonds peaked at 530.8 which is 0.8 eV higher than that of bulk structure and can be due to crystal texturing. Moreover, the peak at 532.8 eV is an indication of non-stoichiometry of oxygen atoms. Zakrzewska attributed this to oxygen atoms at surface states resulting in asymmetry of O1s orbital [16]. They concluded that mostly OH-group chemisorption takes place on unsaturated Ti-sites at the surface such as Ti^{3+} [16]. This conclusion can enhance the molecular (aptamer) adsorption on the surface of TiO_2 structure and increase its potential for biosensing applications. Fig. 2c illustrates Ti 2p orbital scan with peak splitting at 459.2 eV and 464.9 eV. It shows a slight increase (0.1–0.2 eV) of binding energy compare to other reports for TiO_2 anatase nanostructures [17]. This may be due to the crystal growth orientation towards (200) plane. Moreover 5.9 eV energy splitting between $2p_{1/2}$ and $2p_{3/2}$ orbitals shows the attachment of TiO_2 to graphene layers [17]. To examine this idea and to check applicability of hybrid nanosheets, the work

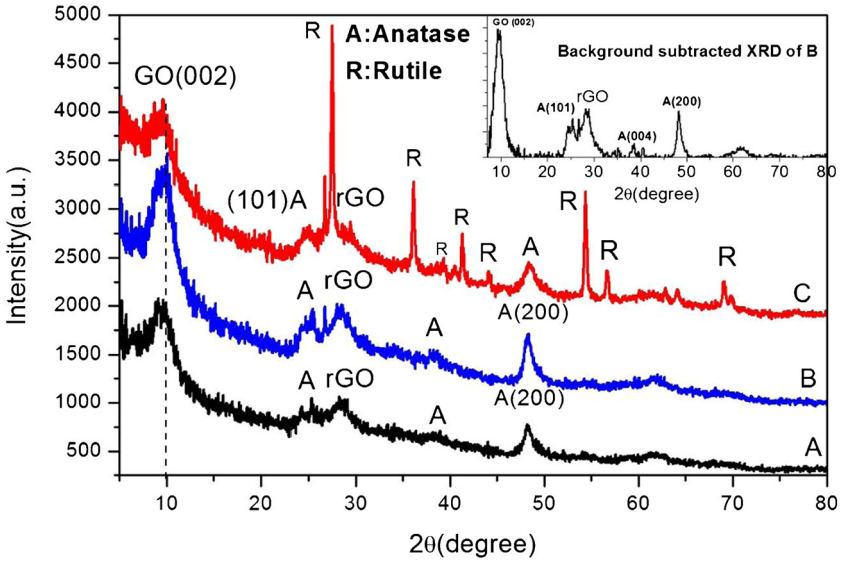

Fig. 1 XRD patterns of samples (**a**) S5, (**b**) S3 and (**c**) S1. Inset shows the XRD pattern of sample S3 with subtracted background. The (200) plane of anatase is the preferential growth plane

function of the samples from graphene side and TiO_2 side were measured. Fig.S12 and Fig. S13 show the work functions for S1 and S5 as noted for graphene side with values roughly about 5.4 and 5.3 eV for S1 and S5, respectively. It is in excellent agreement with the values reported for (reduced) graphene oxide [15]. The slight difference may be due to more reduction of S5 due to the increase of graphene oxide weight and its reduction during hydrothermal process. Moreover, the values of work function for TiO_2 side are roughly 5.3 and 5.2 eV for S1 and S5, respectively. These are higher than the value reported for anatase (101) (5.1 eV) [18]. This can be due to crystal orientation of TiO_2 nanosheets in agreement with 0.2 eV increase of Ti 2p binding energy from XPS analysis. It is noteworthy to say the low difference of work function between graphene side and TiO_2 side

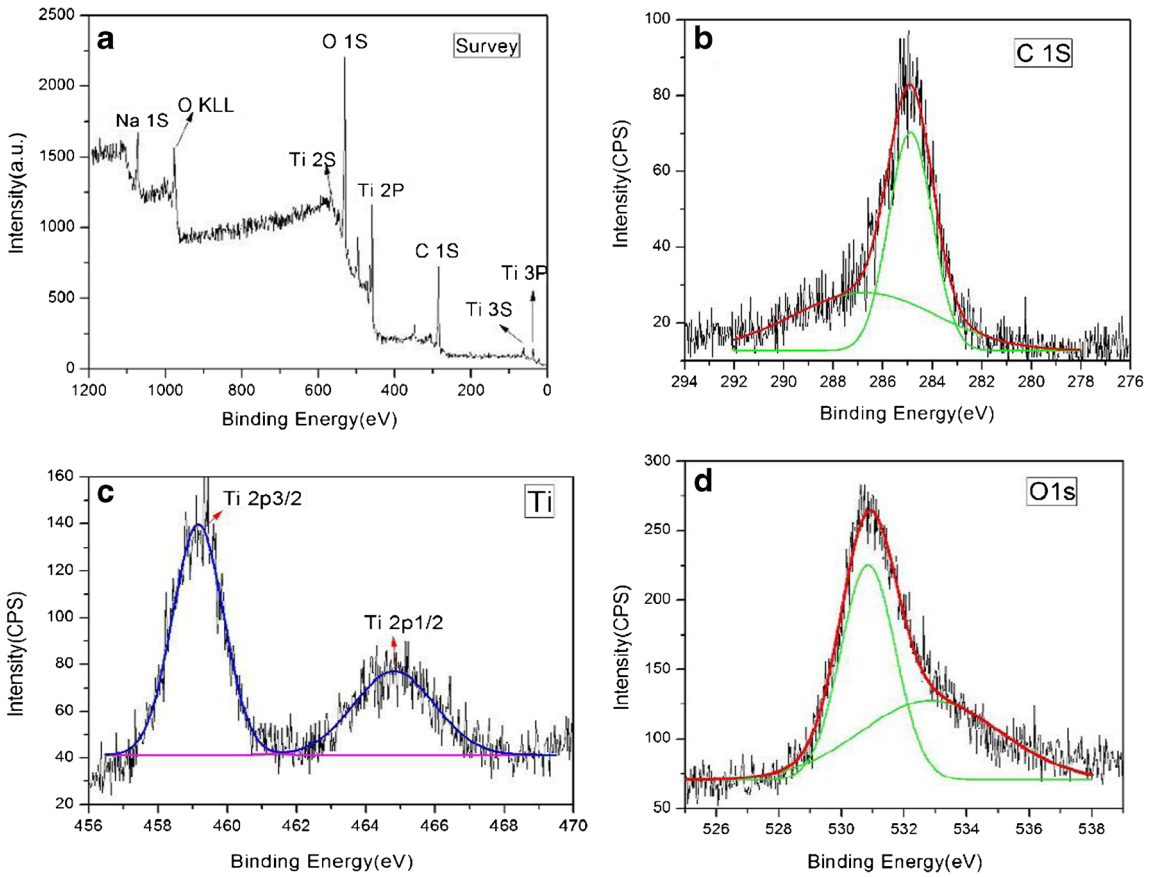

Fig. 2 XPS spectra and deconvolution of S5 sample (**a**) survey scan, (**b**) C 1 s, (**c**) Ti 2p and (d) O 1 s orbital scans

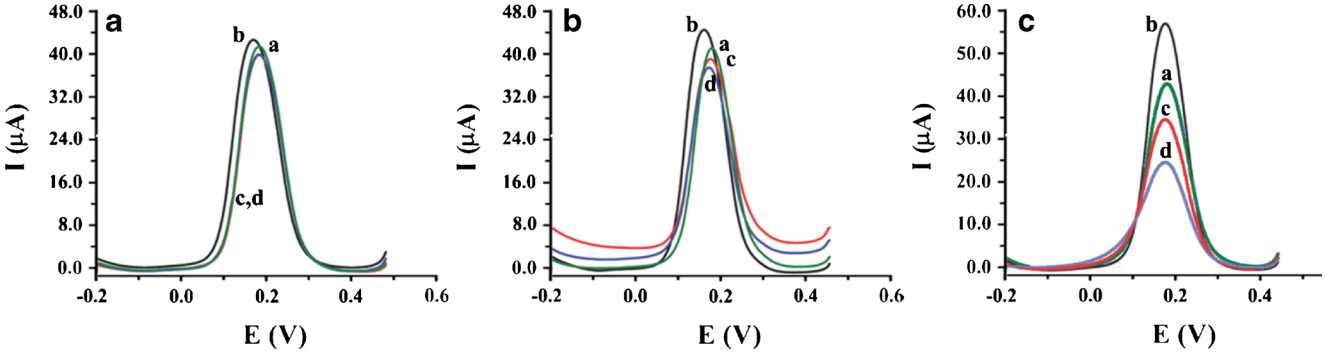

Fig. 3 DP voltammograms of bare GCE (**a**) modified GCEs (**b**), immobilized aptamer on the modified GCEs (**c**), and aptamer coordinated with PSA (3.0 ng mL^{-1}) (**d**). The modified electrodes are (**a**) GO, (**b**) TiO_2, and (**c**) GO- TiO_2. DP curves obtained in a solution containing 3.0 mmol L^{-1} $K_3[Fe(CN)_6]/K_4[Fe(CN)_6]$ (1:1) mixture and 0.1 mol L^{-1} KCl in phosphate buffer (pH 7.0)

(~0.1 eV) can facilitate electron transport through this hybrid structure. Hence, It can raise its potential application as biosensor. Large surface area with a mesoporous structure having several nanometer pore size is a must for the material as the platform of biosensors. Thus, BET-BJH analyses were performed using adsorption-desorption isotherm measurement of samples S1 and S5 (Fig. S14). The results obtain 97 m^2/g and 6–7 nm pore size for S5. Thus it can be quite qualified for high aptamer molecule adsorption.

Detection of PSA by the modified glassy carbon electrode (apt/GO-TiO2/GCE)

The detection effectiveness of the aptasensor was shown in Fig. 3. The figure shows differential pulse voltammograms of 3.0 mmol L^{-1} $K_3[Fe(CN)_6]/K_4[Fe(CN)_6]$ (1:1) mixture on the surface of modified electrodes at different steps for the detection of PSA based on three nanomaterials, i.e., GO (A), TiO_2 (B) and rGO- TiO_2 (C). As shown in the figure, the oxidation peak of $K_4[Fe(CN)_6]$ is observed at approximately 190 mV (vs. Ag/AgCl) on a bare GCE (trace a). After coating of TiO_2 nanocrystals (Fig. 3a, trace b) and GO (Fig. 3b, trace b), the redox current slightly increases, suggesting that the electrode transfer process between $Fe(CN)_6^{3-/4-}$ and electrode surface is enhanced. The GO-TiO_2 modified electrode shows an enhanced oxidation peak current response for $Fe(CN)_6^{3-/4-}$ (Fig. 3c, trace b) when compared to GO and TiO_2 modified electrode, which is clear evidenced the excellent electrocatalytic activity of GO-TiO_2 towards the redox of $[Fe(CN)_6]^{3-/4-}$. It obviously showed that the GO-TiO_2 is fully qualified to act as a great promoter that can accelerate the electrochemical process successfully. After the aptamer were modified on the nanomaterial functionalized electrodes surfaces, the peak current (I_p) decreased in sequence (trace c in Fig. 3a-c) because the aptamer further hindered the electron transfer and greatly reduced the effective area and active sites for electron transfer and prevented the access of electrons to the surface and inhibits interfacial charge-transfer. The curve d (Fig. 3a-c) shows differential pulse voltammograms of 3.0 mmol L^{-1} $K_3[Fe(CN)_6]/K_4[Fe(CN)_6]$ (1:1) mixture upon self-assembly of PSA on the surface of Apt/nanomaterials/GCE modified electrodes. These curves show the current value continue to decrease, indicating that the conductivity continued to decline and hindrance generated by the PSA increase.

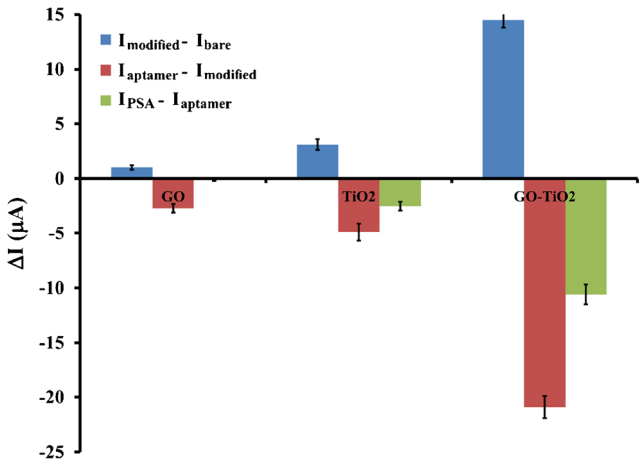

Fig. 4 Variation in I_p for each stage in PSA detection was measured using the biosensors, in which GO, TiO_2, and GO- TiO_2 were used as sensitive layers

In order to evaluate the efficiency of each of the three nanomaterials for PSA detection, a chart (Fig. 4) was prepared where the Y-axis is difference between I_p values after and before the generation of a new layer (ΔI). Concerning the GCEs covered with nanomodifiers, the ΔI values for PSA detection show an increase at all three GO, TiO_2 and GO-TiO_2 modified electrodes, but, this increase is more pronounced for the electrode modified with the GO-TiO_2. The ΔI values of approximately 0, 2.5 and 10.6 μA in the case of GO, TiO_2 and GO-TiO_2 is observed after PSA detection, respectively. It can be concluded that the GO-TiO_2 nanocomposite modified GCE has a superior ability for ultrasensitive detection of PSA. Fig. 5

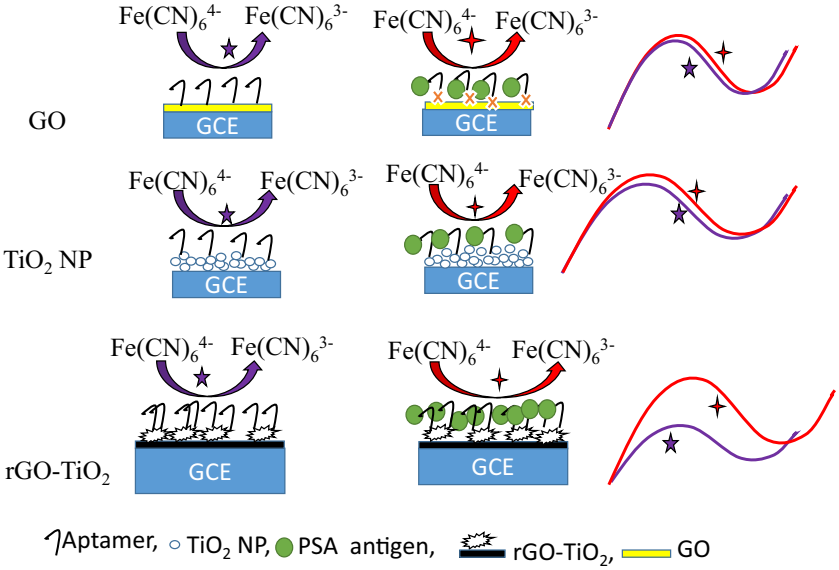

Fig. 5 Comparative schematic of biosensing response to elechtorchemical reaction

shows schematically the dependence of the electrochemical signal on the type of nanomaterials used.

DNA is readily adsorbed on surfaces modified with TiO_2 nanoparticles [18] and GO-contained nanomaterials [13, 19, 20]. It is unclear what mechanism would explain adsorption of DNA onto the TiO_2 nanoparticle surface. However, Zhang and coworkers (2014) reported that the DNA adsorption on the TiO_2 nanoparticles is achieved mainly via the backbone phosphate, while the role of the bases is less important [21]. Therefore, the presence of TiO_2 can enhance the adsorption capacity of the aptamer onto the nanomaterial. As shown in the Fig. 4, a response change is observed after the aptamer immobilized on the surface of TiO_2, and there is an increase of ΔI after the addition of PSA. Moreover, Graphene and its related materials have been described to interact toughly with DNA through hydrophobic and π stacking interactions between the ring structures in the DNA bases and the graphitic domains of graphene [22]. The ΔI of 2.7 μA after immobilization of aptamer on the surface of GO-modified GCE indicate the suitability of GO for aptamer immobilization. But, no significant current change is observed after the addition of PSA as the main response (Fig. 5). It indicates that the PSA is not bonded with the GO/aptamer modified GCE. In other words, the presence of GO can enhance the adsorption ability of the aptamer onto the electrode surfaces, but the PSA cannot interact with aptamer in a proper way. This can be due to a change in the configuration of the aptamer after immobilization on the GO-based materials.

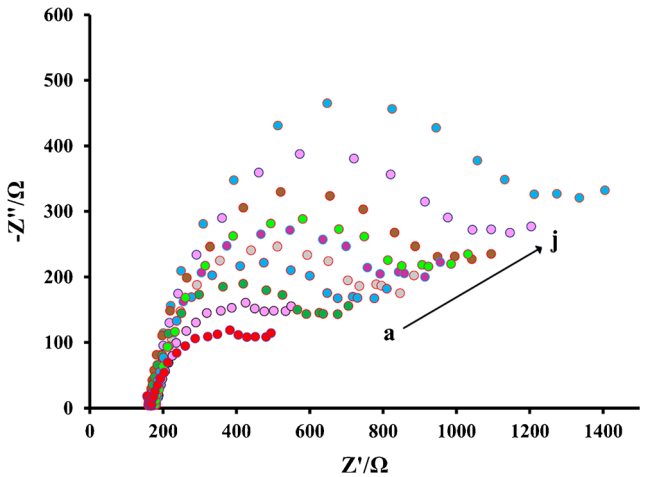

Fig. 6 Nyquist plots of aptamer-immobilized GO-TiO_2 for PSA detection at different concentrations of (**a**) 0.0; (**b**) 0.003; (**c**) 0.01; (**d**) 0.03; € 0.1; (**f**) 0.3; (**g**) 3.0; (**h**) 10.0; (**i**) 30.0, and (**j**) 1000 ng mL^{-1}

The adsorption amount of aptamer enhanced onto the composite electrode modified with the rGO-TiO_2 nanosheets. It seems that the mesoporous morphology of the TiO_2 nanosheets with a huge internal contact area lead to the possibility of a significant increase in the immobilized aptamer on the substrate. Furthermore, this significant increase of current can be due to facile charge transfer to electrode due to promotion of TiO_2 work function and its crystal orientation towards (200) plane as discussed above.

The current responses of GC electrodes modified with the different (S1, S2, S3, S5, S7 and S9) rGO-TiO_2 hybrids were investigated and are shown in Fig. S17. The maximum signal of 10.6 μA is observed for S5/GCE. Therefore, the 5:1 GO-TiO_2 (S5)/GCE is an efficient electrode which is chosen for the upcoming electrochemical measurements of PSA. This interesting results indicate the effect of proximity of GO and TiO_2 sheets that two crucial factors are competitive in aptamer biosensors which has not been modified yet. The TiO_2 islands' compactness and the porosity of hybrid nanosheets. The thickness of TiO_2 accumulated sheets should be such that does not hinder or delay charge transfer to the rGO template while their TiO_2 nanosheet compactness should provide

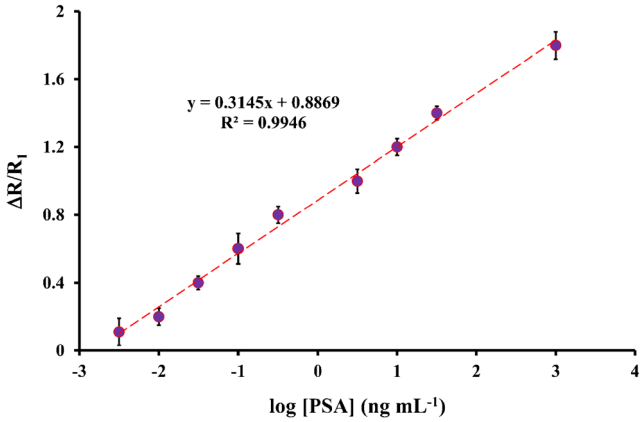

Fig. 7 Linear calibration plot for ΔR/R1 vs. log [PSA] (ng mL^{-1}), where [PSA] is the PSA concentration

enough porosity for attachment of aptamer sensors. These two issues have been resolved in S5.

Figures of merit

The designed S5/GCEs under the optimum conditions were used to detect various concentrations of PSA and their performance. Due to the high sensitivity of EIS to other electrochemical techniques, Nyquist spectra of modified electrode was investigated. The data is fitted well with an equivalent circuit (Fig. S18). This circuit includes the resistive and capacitive elements: Rs is the electrolyte resistance, the constant phase element Q_1 is then related to the space charge capacitance at the electrode| electrolyte interface, Rct is related to the charge transfer resistance at the electrode| electrolyte interface and the constant phase element Q_2 is the Warburg impedance resulting from the diffusion of ions from the bulk of the electrolyte to the interface. As shown in Fig. 6, the impedimetric response of S5/GCE increases with increasing of PSA concentration. Fig. 7 shows the relationship between $\Delta R/R_1$ of S5/GCEs and logarithm of PSA concentration, it can be concluded that the $\Delta R/R_1$ is positively related to logarithm of PSA concentration in the range of 0.003–1000 ng mL^{-1} ($R^2 = 0.9946$). The limit of detection is estimated 1.0 pg mL^{-1}, as calculated at a signal-to-noise ratio of 3, which is defined as PSA concentration corresponding to the signal and is equal to the zero signal minus three times the standard deviation. The remarkable point is that the amount of detection limit obtained using the mentioned method is much less compared with that obtained by other electrochemical methods (Table 1).

To investigate the reproducibility of 5:1GO-TiO_2(S5)/GCE for determination of PSA, seven S5/GCEs were constructed according to the recommended procedure in second and third section and used to determine the 0.3 ng mL^{-1} PSA. The

Table 2 Comparison of proposed aptasensor and Immunoradiometric assay for the detection of PSA in serum

Sample	Obtained value[a] (ng mL^{-1})	Immunoradiometric assay[a] (ng mL^{-1})
A	31.0 ± 1.02	29.67 ± 0.94
B	20.91 ± 0.80	20.02 ± 0.73
C	70.20 ± 1.12	72.12 ± 1.23
D	3.01 ± 0.41	2.89 ± 0.51

[a] Each value is the mean of five replicate experiments

Table 1 Comparison of the analytical performance of different electrochemical systems reported for the PSA detection

Recognition element	Linear range (ng mL^{-1})	Detection limit (pg mL^{-1})	Reference
Apt/rGO-TiO_2(200)/GCE	0.003–1000	1	This work
Aptamer immobilized on the rGO-MWCNT/AuNPs	0.005–100	1	[13]
Aptamer	0.125–200	50	[4]
Aptamer-MIP hybrid receptor	0.1–100	1	[5]
Aptamer	0.007–6	1000	[6]
Hemin-functionalized graphene-palladium nanoparticles	0.025–205	8	[23]
SPCE/MoS_2-QD/PSA_{Ab}	0.00001–200	0.01	[24]
MIP/chit/GS-AuNP/GCE	0.001–100	0.15	[25]
Fe_3O_4-RGO-Ab_1 Pt-Cu-Ab_2	0.00001–5	0.03	[26]
biot-anti-PSA/str/ABA/ nano-TiO2-CPE	0.1–100	200	[27]
Aminated aptamer	1–100	1000	[28]
Au/Cys/Fc-PAMAMs/antiPSA	0.01–100	1	[29]
Aptmaer/AuNPs-graphitized mesoporous carbon	0.25–200	250	[30]
Ab_1-Ag-Ab_2-HRP	0–15	250	[31]

Ab_1-Ag-Ab_2-HRP: Antibody 1-antigene-antibody 2-horseradish peroxidase

RSD% values in this study is achieved 6.9% which represent the good electrode-to-electrode reproducibility.

For the assessment of the aptasensor stability, S5/GCEs were stored at 4 °C under optimal conditions. Then we used them to detect the 0.3 ng mL^{-1} PSA every 5 days up to 30 days. The current response value decreased approximately 4–7%, which further illustrated the good stability and life time of the aptasensor.

Interference study

In order to investigate the effects of some interfering species in the measurement of PSA, before examining the effectiveness of the method in real samples, some species that are structurally similar to PSA were selected and their influence was examined in Tris buffer (pH = 7.0) for measurement of 0.3 ng mL^{-1} PSA. It is found that 50 fold of bovine serum albumin (BSA), hemoglobin, thrombin, human IgG, and lysozyme had not any effect on selectivity (Fig. S19). To further check the selectivity of this aptasensor, the cross-reactivity of other PSA analogues was investigated. As shown in Fig. S20, PSA (0.3 ng mL^{-1}) show a much stronger change in Rct of the aptasensor, while nearly insignificant electrochemical changes are sensed for any of the PSA analogues (15.0 ng mL^{-1}). The results in this section demonstrate that the method is very selective for determination of trace amount of PSA.

Real sample analysis

In order to inspect the effectiveness of constructed biosensor to detect PSA, different serum samples were selected and prepared for analysis according to the recommended procedure in second to sixth section. These samples had previously been used in the diagnosis of prostate cancer. The level of PSA was recognized using the aptasensor and standard immunoradiometric assay used to assess the performance of the biosensor. The results in Table 2 reveal that the method has good ability for analysis of PSA in real samples.

Conclusion

rGO-TiO_2nano hybrids were synthesized by a scalable and cheap hydrothermal method only by incorporation of TiO_2, GO and NaOH powders. No ligand and complex chemical was used for this synthesis. The hybrid nanosheets show a uniformity in physical properties in large scale and are flexible, conductive suitable for sensing and electronic applications. Further, the fabricated rGO-TiO_2 nanosheets was used as electrode modifier for electrochemical aptasensing of PSA. The rGO-TiO_2 biosensor has advantages for biomolecule immobilization, including (i) large surface area, rich π – conjugation structure, and good in-plane conductivity caused by the presence of GO, (ii) a unique porous structure of TiO_2 nanosheets. In conclusion, we were able to demonstrate an effective synergism between GO and TiO_2 in regard to the immobilization of aptamer molecules. Given that the aptasensor shows many advantages such as high sensitivity, selectivity, and stability, this approach can be adapted to aptamer-based detection of other proteins and small molecules. Besides, although the technique was focused on the determination of BPA, it possesses the potential of wider application for other targets. Despite all these advantages, a major limitation of the aptasensor is their relatively costly production.

Compliance with ethical standards The author(s) declare that they have no competing interests.

Publisher's Note Springer Nature remains neutral with regard to jurisdictional claims in published maps and institutional affiliations.

References

1. Rodríguez GA, Díaz-García CV, Agudo-López A, Prieto GE, Ponce S, López-Martín JA, Paz-Ares L, Iglesias L, Agulló-Ortuño MT (2016) Blood-based biomarkers for monitoring antiangiogenic therapy in non-small cell lung cancer. Med Oncol 33:105
2. Hori SS, Lutz AM, Paulmurugan R, Gambhir SS (2017) A model-based personalized cancer screening strategy for detecting early-stage tumors using blood-borne biomarkers. Cancer Res 77:2570–2584
3. Damborska D, Bertok T, Dosekova E, Holazova A, Lorencova L, Kasak P, Tkac J (2017) Nanomaterial-based biosensors for detection of prostate specific antigen. Microchim Acta 184(9):3049–3067. https://doi.org/10.1007/s00604-017-2410-1
4. Rahi A, Sattarahmady N, Heli H (2016) Label-free electrochemical aptasensing of the human prostate-specific antigen using gold nanospears. Talanta 156-157:218–224. https://doi.org/10.1016/j.talanta.2016.05.029
5. Pawan J, Formisano N, Tkac J, Kasák P, Frost CG, Estrela P (2015) Label-free Impedimetric Aptasensor with antifouling surface chemistry: a prostate specific antigen case study. Sensors Actuators B Chem 209:306–312. https://doi.org/10.1016/j.snb.2014.11.083
6. Pawan J, Tamboli V, Harniman RL, Estrela P, Allender CJ, Bowen JL (2016) Aptamer-MIP hybrid receptor for highly sensitive electrochemical detection of prostate specific antigen. Biosens Bioelectron 75:188–195. https://doi.org/10.1016/j.bios.2015.08.043
7. Kong RM, Ding L, Wang Z, You Qu JF (2015) A novel aptamer-functionalized MoS2 nanosheet fluorescent biosensor for sensitive detection of prostate specific antigen. Anal Bioanal Chem 407:369–377. https://doi.org/10.1007/s00216-014-8267-9
8. Meirinho SG, Dias LG, Peresd AM, Lígi RR (2016) Voltammetric aptasensors for protein disease biomarkers detection: a review. Biotechnol Adv 34(5):941–953. https://doi.org/10.1016/j.biotechadv.2016.05.006
9. Zhou L, Wang J, Li D, Li Y (2014) An electrochemical aptasensor based on gold nanoparticles dotted graphene modified glassy carbon electrode for label-free detection of bisphenol a in milk samples. Food Chem 162:34–40. https://doi.org/10.1016/j.foodchem.2014.04.058
10. Liu Y, Liu Y, Liu B (2016) A dual-signaling strategy for ultrasensitive detection of bisphenol a by aptamer-based electrochemical

biosensor. J Electroanal Chem 781:265–271. https://doi.org/10.1016/j.jelechem.2016.06.048
11. Zhu Y, Zhou C, Yan X, Yan Y, Wang Q (2015) Aptamer-functionalized nanoporous gold film for high-performance direct electrochemical detection of bisphenol a in human serum. Anal Chim Acta 883:81–89. https://doi.org/10.1016/j.aca.2015.05.002
12. Huang Y, Li X, Zheng S (2016) A novel and label-free immunosensor for bisphenol a using rutin as the redox probe. Talanta 160:241–246. https://doi.org/10.1016/j.talanta.2016.07.017
13. Heydari-Bafrooei E, Shamszadeh NS (2017) Electrochemical bioassay development for ultrasensitive aptasensing of prostate specific antigen. Biosens Bioelectron 91:284–292
14. Kasuga T, Hiramatsu M, Hoson A, Sekino T, Niihara K (1999) Titania nanotubes prepared by chemical processing. Adv Mater 11:1307–1311
15. Zheye Z, Fei X, Yunlong G, Shuai W, Yunqi L (2013) One-pot self-assembled three-dimensional TiO2-graphene hydrogel with improved adsorption capacities and photocatalytic and electrochemical activities. ACS Appl Mater Interfaces 5(6):2227–2233. https://doi.org/10.1021/am303299r
16. Zakrzewska K (2011) Nonstoichiometry in TiO2−y studied by ion beam methods and photoelectron spectroscopy. Adv Mater Sci Eng 2012:13–13. https://doi.org/10.1155/2012/826873
17. Zhang H, Panpan X, Guidong D, Chen Z, Kokyo O, Pan D, Jiao Z (2011) A facile one-step synthesis of TiO2/graphene composites for Photodegradation of methyl Orange. Nano Res 4(3):274–283. https://doi.org/10.1007/s12274-010-0079-4
18. David OS, Charles WD, John B, Stephen AS, Andrew JL, Scott MW, Richard C, AC MJP, Robert GP, Ivan PP, Graeme WW, Thomas WK, Paul S, Aron W, Alexey AS (2013) Band alignment of rutile and Anatase TiO2. Nat Mater 12:798–801. https://doi.org/10.1038/NMAT3697
19. Amano T, Toyooka T, Ibuki Y (2010) Preparation of DNA-adsorbed TiO2 particles–augmentation of performance for environmental purification by increasing DNA adsorption by external pH regulation. Sci Total Environ 408(3):480–485. https://doi.org/10.1016/j.scitotenv.2009.10.037
20. Xu Y, Wu Q, Sun Y, Bai H, Shi G (2010) Three-dimensional self-assembly of graphene oxide and DNA into multifunctional hydrogels. ACS Nano 4(12):7358–7362. https://doi.org/10.1021/nn1027104
21. Wang M, Zhai S, Ye Z, He L, Peng D, Feng X, Yang Y, Fang S, Zhang H, Zhang Z (2015) An electrochemical aptasensor based on a TiO2/three-dimensional reduced graphene oxide/PPy nanocomposite for the sensitive detection of lysozyme. Dalton Trans 44(14):6473–6479. https://doi.org/10.1039/c5dt00168d
22. Xu Z, Feng W, Liu B, Erin YK, Mark RS, Liu J (2014) Adsorption of DNA oligonucleotides by titanium dioxide nanoparticles. Langmuir 30:839–845. https://doi.org/10.1021/la404633p
23. Zhang G, Liu Z, Fan L, Guo Y (2018) Electrochemical prostate specific antigen aptasensor based on hemin functionalized graphene-conjugated palladium nanocomposites. Microchim Acta 185(3):159. https://doi.org/10.1007/s00604-018-2686-9
24. Kukkar M, Singh S, Kumar N, Tuteja SK, Kim KH, Deep A (2017) Molybdenum disulfide quantum dot based highly sensitive impedimetric immunoassay for prostate specific antigen. Microchim Acta 184(12):4647–4654. https://doi.org/10.1007/s00604-017-2506-7
25. Ma Y, Shen XL, Zeng Q, Wang LS (2017) A glassy carbon electrode modified with graphene nanoplatelets, gold nanoparticles and chitosan, and coated with a molecularly imprinted polymer for highly sensitive determination of prostate specific antigen. Microchim Acta 184(11):4469–4476. https://doi.org/10.1007/s00604-017-2458-y
26. Jiao L, Mu Z, Miao L, Du W, Wei Q, Li H (2017) Enhanced amperometric immunoassay for the prostate specific antigen using Pt-cu hierarchical trigonal bipyramid nanoframes as a label. Microchim Acta 184(2):423–429. https://doi.org/10.1007/s00604-016-2023-0
27. Biniaz Z, Mostafavi A, Shamspur T, Torkzadeh-Mahani M, Mohamadi M (2017) Electrochemical sandwich immunoassay for the prostate specific antigen using a polyclonal antibody conjugated to thionine and horseradish peroxidase. Microchim Acta 184(8):2731–2738. https://doi.org/10.1007/s00604-017-2284-2
28. Souada M, Piro B, Reisberg S, Anquetin G, Noël V, Pham MC (2015) Label-free electrochemical detection of prostate-specific antigen based on nucleic acid aptamer. Biosens Bioelectron 68:49–54. https://doi.org/10.1016/j.bios.2014.12.033
29. Çevik E, Bahar Ö, Şenel M, Abasıyanık MF (2016) Construction of novel electrochemical immunosensor for detection of prostate specific antigen using ferrocene-PAMAM dendrimers. Biosens Bioelectron 86:1074–1079. https://doi.org/10.1016/j.bios.2016.07.064
30. Liu B, Lu L, Hua E, Jiang S, Xie G (2012) Detection of the human prostate-specific antigen using an aptasensor with gold nanoparticles encapsulated by graphitized mesoporous carbon. Microchim Acta 178(1–2):163–170
31. Sarkar P, Pal PS, Ghosh D, Setford SJ, Tothill IE (2002) Amperometric biosensors for detection of the prostate cancer marker (PSA). Int J Pharm 238:1–9